Study of the Origin of Short- and Long-latency SSEP during Recovery from Brain Ischemia in a Rat Model

Dan Wu[a], **Bezerianos Anastassios**[a,c], **Wei Xiong**[b], **Jai Madhok**[a], **Xiaofeng Jia**[a,d], and **Nitish V. Thakor**[a,*]

[a] Department of Biomedical Engineering, Johns Hopkins University, Baltimore, MD 21205, USA

[b] Department of Neurology, Johns Hopkins University School of Medicine, Baltimore, MD 21287, USA

[c] Department of Medical Physics, School of Medicine, University of Patras, 26500 Patras, Greece

[d] Department of Physical Medicine and Rehabilitation, Johns Hopkins University School of Medicine, Baltimore, MD 21205, USA

Abstract

Somatosensory evoked potentials (SSEPs) have been established as an electrophysiological tool for the prognostication of neurological outcome in patients with hypoxic-ischemic brain injury. The early and late responses in SSEPs reflect the sequential activation of neural structures along the somatosensory pathway. This study reports that the SSEP can be separated into early (short-latency, SL) and late (long-latency, LL) responses using Independent Component Analysis (ICA), based on the assumption that these components are generated from different neural sources. Moreover, this source separation into the SL and LL components allows analysis of electrophysiological response to brain injury, even when the SSEPs are severely distorted and SL and LL components get mixed. With the help of ICA decomposition and corrected peak estimation, the latency of LL-SSEP is shown to be predictive of long-term neurological outcome. Further, it is shown that the recovery processes of SL- and LL-SSEPs follow different dynamics, with the SL-SSEP restored earlier than LL-SSEP. We predict that the SL- and LL-SSEPs reflect the timing of the progression of evoked response through the thalamocortical pathway and as such respond differently depending upon injury and recovery of the thalamic and cortical regions, respectively.

Keywords

Somatosensory Evoked Potential; short/long-latency; brain ischemia; Independent Component Analysis; thalamocortical

Introduction

Somatosensory Evoked Potentials (SSEPs) consist of a series of waves generated from the sequential activation of neural structures along the somatosensory pathway. Yet there is no

clear view about the mapping of SSEP peaks with their origins. The SSEP waveform is conventionally viewed as comprised of two components—the short-latency (SL) and the long-latency (LL) complexes. Researchers have looked into SL and LL complex in humans, and established the SL-peak N20 as an indicator of thalamocortical integrity and the LL-peak N70 as an indicator of cortical function [23], with a general understanding of SL-SSEP to be a thalamocortical response and LL-SSEP to be a corticocortical response [7]. There have been subjective definitions of short/middle/long-latencies [8,10,23], but the justifications for such definitions are unclear. Simple time-domain segmentation may lose its power when the signals are not standard and highly variable which is often the case when SSEPs are recorded from injured brain. Therefore, a more universal and justified segmentation approach is needed to assist the analysis of SSEPs.

In this paper we study the SL- and LL-SSEPs during recovery from brain ischemia in a rat model of asphyxial cardiac arrest (CA) [12]. In view of the association of SL and LL responses in SSEP with their thalamocortical origins, it is expected that the separation of SL- and LL-SSEP would shed insights into diagnosis and prognosis of different levels of brain injury. Here, we present an innovative way of separating SL- and LL-SSEPs using Independent Component Analysis (ICA), based on the assumption that they are generated from different sources and can thus be considered statistically independent.

ICA has been a well-established method for blind source separation in various neural signals [24–26], for example, ICA components have been used in dipole source modeling to find the source underlying surface EEG recordings [21]. Therefore, we expect ICA to decompose the inputs of multichannel SSEP recordings into the SL and LL components of different sources. The remainder of this paper discusses the effectiveness of using ICA for SSEP segmentation, along with the advantages and limitations of this method.

Materials and Methods

Experiment

Our experimental studies are motivated by the problem of assessing the neural electrophysiological changes as a result of global ischemia following cardiac arrest (CA). The experiment protocol was approved by the Johns Hopkins Animal Care and Use Committee. Sixteen male Wistar rats (350±25g) were subjected to either a 7min (n=8) or 9min (n=8) of asphyxia. Rats were mechanically ventilated with 1.5% isoflurane in a 50:50% N_2/O_2 gas mixture. The femoral artery and vein distal to the inguinal ligament were cannulated in order to monitor mean arterial pressure (MAP), sample arterial blood gas (ABG) and administer drugs. Body temperature was maintained within normal values 36.5–37.5°C throughout the experiment. After a 15min baseline recording, the isoflurane was washed out for 5min to eliminate the residual effect of anesthesia. 2mg/kg of vecuronium was infused 2min after washout and the gas mixture was switched to room air. CA was initiated with cessation of mechanical ventilation and lasted for 7 or 9min, as predetermined. Cardiopulmonary resuscitation (CPR) was performed with external chest compressions, mechanical ventilation, and infusion of epinephrine and $NaHCO_3$ until return of spontaneous circulation (ROSC). Isoflurane was restarted at 0.5% after 45min to maintain animal comfort during SSEP recording.

One week prior to CA, rats were implanted with 4 epidural screw electrodes (Plastics One, Roanoke, VA) on the left (chA, chC) and right (chB, chD) somatosensory cortex, along with a ground in the parasagittal right frontal lobe. Median nerve stimulation was given alternatively through needle electrodes in the right and left distal forelimbs with 200μs-long 0.6mA pulses delivered at 0.5 Hz. The SSEPs were recorded using the TDT data acquisition system (Tucker Davis Technologies, Alachua, FL) at 6.1k Hz, and the first 150ms signals

post-stimulus were recorded and analyzed. Signals were recorded continuously for 1hr after onset of CA, intermittently for the next 3hrs with 15min rest periods, and for 15mins at 24hr, 48hr and 72hr after ROSC.

The neurological outcome after CA is determined by an extensive neurological examination using the Neurological Deficit Score (NDS). The NDS, ranging from 80 (best) to 0 (brain dead) was previously developed and validated by us [11,12,15,16].

Methods

ICA is implemented to separate the SL and LL complexes of the SSEP. The ICA is a method for solving the blind source separation problem, which aims to find a linear coordinate system such that the constituent signals derived from a mixture are as statistically independent from each other as possible [20]. Assume that there are m independent source signals $s = (s_1,\ldots,s_m)$, being observed in n channels $x = (x_1,\ldots,x_n)$, then the ICA model is defined as [5] $x = \mathbf{A}s$ with a mixing matrix $\mathbf{A}$, and a demixing matrix $\mathbf{W}$ to estimate the underlying sources $u = \mathbf{W}x$. The adaptive algorithms for $\mathbf{W}$ have been derived from many criteria [14]. The particular model used in this study was proposed by Bell and Sejnowski [3] using information maximization (Infomax). We choose Infomax ICA because it is more robust to sources that are not strictly independent and it is more tolerant to noise, than other ICA methods such as fastICA [13]. The Infomax ICA algorithm is essentially a feed-forward neural network designed with a nonlinear transformation $y_i = g_i(u_i)$ after the linear transformation from x to u The goal of Infomax is to maximize the joint entropy $H(y_1, \ldots, y_n)$, and $\mathbf{W}$ is recursively adjusted [2] towards the maximization of $H(y)$.

Here, Infomax ICA is implemented by taking two channels of SSEPs on the same hemisphere (chA/C or chB/D) from the somatosensory cortex as input vector and giving outputs of two independent components (ICs)—the short-latency IC (SLIC) and long-latency IC (LLIC) component. The Infomax procedure is executed using EEGLAB Matlab toolbox [6].

For preprocessing, SSEP signals are low-pass filtered with a cutoff frequency of 150Hz and then averaged over 20 sweeps to improve the signal-to-noise ratio (SNR). The use of epidural electrodes bypasses the cranial filtering, thereby records a less damped signal than clinically used scalp recordings. We consider an average over 20 sweeps to be sufficient to obtain a stable signal with a high SNR for analysis. After filtering and averaging, a typical SSEP waveform consists of N10/P15 and N30/P60 complexes in the SL and LL ranges, respectively

Results

An illustration of ICA decomposition of baseline SSEP signals is shown in Fig. 1(A). It is self-explanatory that the ICs, transformed from chA and chC recordings, correspond to SL and LL components, respectively. In SLIC, the N10/P15 complex is emphasized with flattened late responses, whereas in LLIC, the N30/P60 complex became prominent with blurred early responses. This pattern of separation and grouping is consistently observed across subjects in our cohort of animals.

The separation of short and long latencies shows its importance during early recovery from brain ischemia induced by CA. The SSEP waveforms can be severely distorted due to the injury with some typical peaks missing and some unexpected peaks emerging. Some SSEP peaks are so small that they are overridden by the preceding or following peaks. The observed delay of these peaks makes the situation even worse—delayed SL-peaks can be mixed or overlapped with LL-peaks. Therefore, early peak detection is technically difficult

with a high probability of false detection. ICA improves peak detection in three ways: it 1) highlights LL-SSEP which is subtle compared to SL-SSEP in raw recordings (Fig. 1(A)), 2) retrieves small peaks which are missing from the raw observations, and 3) minimizes the mutual interference between the SL and LL complex to obtain the true waveforms for SL and LL alone, as evidenced in Fig. 1(B). These improvements are not trivial but significant when we test the prognostic value of SSEP after ICA versus that before ICA, as demonstrated below.

Based on the LL-SSEP separated from ICA analysis, delays of the LL-peaks N30 and P60 at 30, 60, 90, 120, 150, 180, 210 and 240 minutes post-CA were measured, where delay refers to the difference between the prolonged latency and the baseline latency. The rats were divided to good-outcome (n=9) and bad-outcome (n=7) groups according to their NDS evaluated at 72hr after CA. The mean and standard deviation of delays for the two groups are shown in Fig. 2(A) (B). Both N30 and P60 have significantly higher delays for the poorly-recovered rats ($p <0.05$, Student's t-test) than the well-recovered rats at most timeframes. The correlations between the delays and NDS are significant at all timeframes after 30min after CA ($p<0.05$, n=16, Pearson's correlation). However, if the same peak detection was performed on raw SSEPs, delays of N30 and P60 did not show much differences (Fig. 2(C) (D)), possibly due to the distortion of waveforms which gave erroneous detections. The latencies of SL-peaks N10 and P15 are not significantly different between the outcome groups using either the raw SSEPs or decomposed ICs.

One benefit of ICA is that it facilitates the investigation of SL- and LL-SSEPs separately. Fig. 3 shows the evolution of SLIC and LLIC during the first four hours of recovery after CA. Distortions in both SL and LL components were observed early in the recovery, both of which gradually restored towards the baseline as the rat recovered. Along with the change of waveforms, the latencies of SSEP peaks changed from large delays to near baseline values, however, the changing patterns of SL and LL were different. For example, the latency of SL-peak N10 approximately follows an exponential trend which drops at the beginning and stabilizes at about 1hr post-CA; whereas the latency of LL-peak P60 decreases slowly and linearly over time (Fig. 4). Latencies are normalized with respect to the baseline values for comparison, but it is worth noting that the absolute delay of P60 is much greater than that of N10 as shown in the inset figure. These observations point to different recovery dynamics of SL- and LL-SSEPs, and further suggest different vulnerabilities of their neural sources to hypoxic-ischemic insults.

Discussion

The primary somatosensory cortex receives inputs from the thalamus, particularly, the ventral posterior medial (VPM) and ventral posterior lateral (VPL) nuclei as the principal thalamic relays [17]. Cortical layer IV is the major lamina for thalamocortical interaction, which then transmits the sensory information to layer II and upper layer III, where corticocortical communication takes place [19]. The idea that the early and late responses in SSEP are generated in different neural sources drives the motivation for the separation of SL- and LL-SSEPs. Animal studies with spike correlation analysis showed a range of thalamocortical delays from 0.1 to 5ms and corticothalamic delays from 1 to 30ms in the mouse [22,28] and rat [1,29]. Muthuswamy et al. [27] showed an inhibition period in the thalamic multi-unit activity from 30 to 100 ms after onset of stimulus, so that the LL-SSEP during 30–100ms could not have a thalamic origin as the SL-SSEP does. Hence the segmentation of SL- and LL-SSEP around 30ms by ICA (Fig. 1) agrees well with the expected timing of thalamocortical information flow.

ICA separates source signals according to their statistical independence, regardless of the morphology of the waveform, which establishes it as a generic method applicable on any evoked potentials for separation of SL and LL responses. However, one should keep in mind that SL- and LL-SSEPs are not completely independent of each other, as they are driven by the same stimulus. Consequently, we can see residuals of N10/P15 in the LL component after decomposition. It turns out that SL and LL-SSEPs are more separable in injured SSEPs than baseline (Fig. 3), possibly due to the dissociation between thalamic and cortical activities [27]. The drawback of ICA lies in that the amplitude information is lost in the decomposed signals. Nevertheless, latency is generally considered more reliable marker than amplitude for clinical use [30].

In clinical practice, the delay of SL-SSEP reliably predicts poor neurologic outcome [4], but it has a low sensitivity for favorable outcomes. LL-SSEP may hold more promise in predicting good outcomes, but they have poor reproducibility and have not been adequately studied [31]. Thus, there is a need for improved peak detection of LL-SSEP, and the application of ICA provides a solution. Better prognostication is achieved using the separated LL-SSEP by ICA, as shown by the statistical analysis. The LL-SSEP is of particular interest in this study not only because of its prognostic value but also because of its greater vulnerability to brain ischemia. Compared to SL-SSEP, the delay of LL-SSEP after CA is substantial and it takes a longer time to get fully restored (Fig. 4). Assuming its corticocortical generator, the greater vulnerability of the LL-SSEP is supported by histological [18] and MR spectroscopic [9] studies that the cerebral cortex is more sensitive to reduced cerebral blood flow compared to deep brain regions.

The separability of SL and LL responses as independent components, and their different recovery dynamics and vulnerabilities all support the hypothesis that SL- and LL-SSEP are generated by different neural sources. However, in order to fundamentally find out the origins of SL and LL-SSEPs, simultaneous thalamocortical multi-unit recordings from the neural population in both thalamus and cortex and additional correlation analysis will be needed.

Conclusion

ICA is implemented to separate the SL- and LL-SSEP as two components, which are believed to be generated from different neural sources. The separation reduces the interference between SL and LL and thus facilitates peak detection in injured brain. With improved peak detection, the LL-peak latencies are shown to be predictive of long-term outcomes after asphyxial cardiac arrest. The loss and return of SL and LL, which exhibit different dynamics in the recovery during brain ischemia, presumably reflects the functionality of their sources of origin. This study suggests separate origins of SL- and LL-SSEP and this result could be important to the understanding of the role of different neural regions during their recovery from cerebral ischemia.

Acknowledgments

References

1. Beierlein M, Connors BW. Short-term dynamics of thalamocortical and intracortical synapses onto layer 6 neurons in neocortex. J Neurophysiol. 2002; 88:1924–1932. [PubMed: 12364518]

2. Bell AJ, Sejnowski TJ. The "independent components" of natural scenes are edge filters. Vision Res. 1997; 37:3327–3338. [PubMed: 9425547]

3. Bell AJ, Sejnowski TJ. An information-maximization approach to blind separation and blind deconvolution. Neural Comput. 1995; 7:1129–1159. [PubMed: 7584893]

4. Chen R, Bolton CF, Young B. Prediction of outcome in patients with anoxic coma: a clinical and electrophysiologic study. Crit Care Med. 1996; 24:672–678. [PubMed: 8612421]

5. Comon P. Independent component analysis, a new concept? Signal Processing. 1994; 36:287–314.

6. Delorme A, Makeig S. EEGLAB: an open source toolbox for analysis of single-trial EEG dynamics including independent component analysis. J Neurosci Methods. 2004; 134:9–21. [PubMed: 15102499]

7. Doherty, RD.; Hutchison, SJ. The Central Nervous System in Pediatric Critical Illness and Injury. Springer London; London: 2009. p. 1-12.

8. Ellingson BM, Kurpad SN, Schmit BD. Characteristics of mid- to long-latency spinal somatosensory evoked potentials following spinal trauma in the rat. J Neurotrauma. 2008; 25:1323–1334. [PubMed: 18976168]

9. Falini A, Barkovich AJ, Calabrese G, Origgi D, Triulzi F, Scotti G. Progressive brain failure after diffuse hypoxic ischemic brain injury: a serial MR and proton MR spectroscopic study. AJNR Am J Neuroradiol. 1998; 19:648–652. [PubMed: 9576649]

10. Finazzi-Agro E, Rocchi C, Pachatz C, Petta F, Spera E, Mori F, Sciobica F, Marfia GA. Percutaneous tibial nerve stimulation produces effects on brain activity: study on the modifications of the long latency somatosensory evoked potentials. Neurourol Urodyn. 2009; 28:320–324. [PubMed: 19090588]

11. Geocadin RG, Ghodadra R, Kimura T, Lei H, Sherman DL, Hanley DF, Thakor NV. A novel quantitative EEG injury measure of global cerebral ischemia. Clin Neurophysiol. 2000; 111:1779–1787. [PubMed: 11018492]

12. Geocadin RG, Muthuswamy J, Sherman DL, Thakor NV, Hanley DF. Early electrophysiological and histologic changes after global cerebral ischemia in rats. Mov Disord. 2000; 15(Suppl 1):14–21. [PubMed: 10755267]

13. Glass K, Frishkoff GA, Frank RM, Davey C, Dien J, Maloney AD, Tucker DM. A framework for evaluating ICA methods of artifact removal from multichannel EEG. Lect Notes Comput Sc. 2004; 3195:1033–1040.

14. Hyvarinen A, Oja E. Independent component analysis: algorithms and applications. Neural Networks. 2000; 13:411–430. [PubMed: 10946390]

15. Jia X, Koenig MA, Shin HC, Zhen G, Pardo CA, Hanley DF, Thakor NV, Geocadin RG. Improving neurological outcomes post-cardiac arrest in a rat model: immediate hypothermia and quantitative EEG monitoring. Resuscitation. 2008; 76:431–442. [PubMed: 17936492]

16. Jia X, Koenig MA, Shin HC, Zhen G, Yamashita S, Thakor NV, Geocadin RG. Quantitative EEG and neurological recovery with therapeutic hypothermia after asphyxial cardiac arrest in rats. Brain Res. 2006; 1111:166–175. [PubMed: 16919609]

17. Jones EG. The thalamic matrix and thalamocortical synchrony. Trends Neurosci. 2001; 24:595–601. [PubMed: 11576674]

18. Katz L, Ebmeyer U, Safar P, Radovsky A, Neumar R. Outcome model of asphyxial cardiac arrest in rats. J Cereb Blood Flow Metab. 1995; 15:1032–1039. [PubMed: 7593335]

19. Koralek KA, Olavarria J, Killackey HP. Areal and laminar organization of corticocortical projections in the rat somatosensory cortex. J Comp Neurol. 1990; 299:133–150. [PubMed: 2172324]

20. Lee, TW. Independent component analysis: theory and applications. Kluwer Academic Publishers; Boston: 1998.

21. Lelic D, Gratkowski M, Valeriani M, Arendt-Nielsen L, Drewes AM. Inverse modeling on decomposed electroencephalographic data: a way forward? J Clin Neurophysiol. 2009; 26:227–235. [PubMed: 19584750]

22. Liu XB, Bolea S, Golshani P, Jones EG. Differentiation of corticothalamic and collateral thalamocortical synapses on mouse reticular nucleus neurons by EPSC amplitude and AMPA receptor subunit composition. Thalamus and Related Systems. 2001; 1:15–29.

23. Madl C, Grimm G, Kramer L, Yeganehfar W, Sterz F, Schneider B, Kranz A, Schneeweiss B, Lenz K. Early prediction of individual outcome after cardiopulmonary resuscitation. Lancet. 1993; 341:855–858. [PubMed: 8096562]

24. Maeda S, Inagaki S, Kawaguchi H, Song WJ. Separation of signal and noise from in vivo optical recording in Guinea pigs using independent component analysis. Neurosci Lett. 2001; 302:137–140. [PubMed: 11290406]

25. Makeig S, Jung TP, Bell AJ, Ghahremani D, Sejnowski TJ. Blind separation of auditory event-related brain responses into independent components. Proc Natl Acad Sci U S A. 1997; 94:10979–10984. [PubMed: 9380745]

26. McKeown MJ, Jung TP, Makeig S, Brown G, Kindermann SS, Lee TW, Sejnowski TJ. Spatially independent activity patterns in functional MRI data during the stroop color-naming task. Proc Natl Acad Sci U S A. 1998; 95:803–810. [PubMed: 9448244]

27. Muthuswamy J, Kimura T, Ding MC, Geocadin R, Hanley DF, Thakor NV. Vulnerability of the thalamic somatosensory pathway after prolonged global hypoxic-ischemic injury. Neuroscience. 2002; 115:917–929. [PubMed: 12435429]

28. Salami M, Itami C, Tsumoto T, Kimura F. Change of conduction velocity by regional myelination yields constant latency irrespective of distance between thalamus and cortex. Proc Natl Acad Sci U S A. 2003; 100:6174–6179. [PubMed: 12719546]

29. Sawyer SF, Young SJ, Groves PM, Tepper JM. Cerebellar-responsive neurons in the thalamic ventroanterior-ventrolateral complex of rats: in vivo electrophysiology. Neuroscience. 1994; 63:711–724. [PubMed: 7898672]

30. Spiess M, Schubert M, Kliesch U, Halder P. Evolution of tibial SSEP after traumatic spinal cord injury: baseline for clinical trials. Clin Neurophysiol. 2008; 119:1051–1061. [PubMed: 18343719]

31. Wijdicks EF, Hijdra A, Young GB, Bassetti CL, Wiebe S. Practice parameter: prediction of outcome in comatose survivors after cardiopulmonary resuscitation (an evidence-based review): report of the Quality Standards Subcommittee of the American Academy of Neurology. Neurology. 2006; 67:203–210. [PubMed: 16864809]
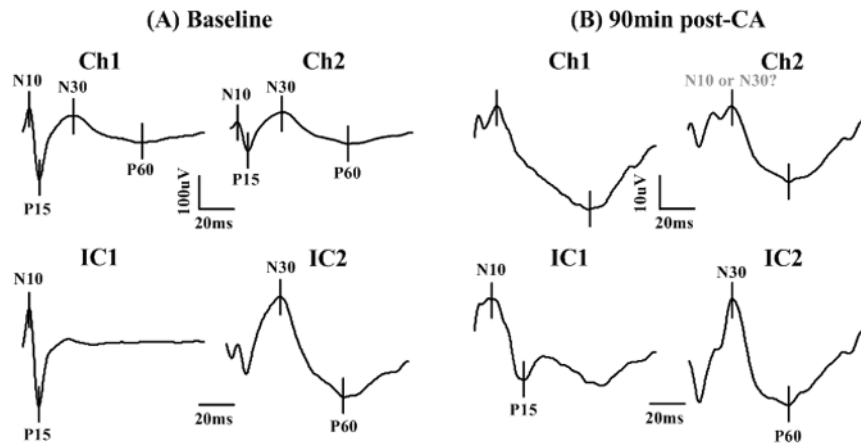
Fig. 1.
ICA decomposition of SSEPs into short- and long-latency components at baseline (A) and after cardiac arrest (B) in a typical CA experiment. The upper two panels in (A) and (B) are two channels of SSEPs recordings, and the lower two panels are the ICA- decomposed independent components (ICs), corresponding to SL- and LL-SSEPs. The SSEPs are averaged over 20 sweeps to improve SNR. The ICA transformed signals are in arbitrary units. Notice that 1) the slow and flat LL complex N30/P60 is magnified in IC2; 2) in (B), the injured SSEP, the P15 peak is missing from the raw data but shows up in IC1; 3) the N10 and N30 peaks are ambiguous in the raw data, whereas after decomposition, the SL and LL components are distinct and peaks are easier to identify.
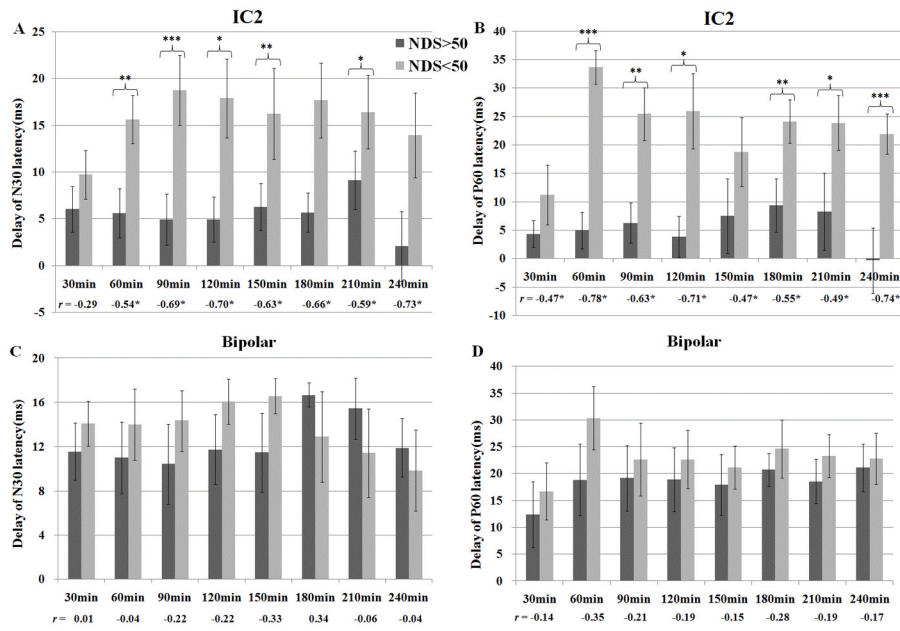
Fig. 2.
Delay of N30 (A) and P60 (B) on the ICA-decomposed long-latency component for the good-outcome and poor-outcome groups at 30, 60, 90, 120, 150, 180, 210, 240 min after CA. The outcomes were determined by the Neurological Deficit Score (NDS), measured at 72hr after CA. *p*-values are derived from the one-tailed Student's *t*-test with unequal variance assumption (*p<0.05, **p<0.02, ***p<0.01). Pearson's correlation coefficient *r* between the delays and NDS at each time frame is shown below the bars with those statistically significant *r* values marked with stars.
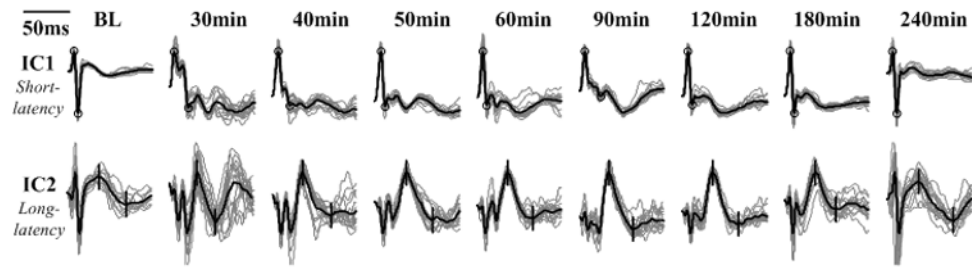
Fig. 3.
Evolution of IC1 (SL-component) and IC2 (LL-component) during recovery from CA in a typical CA experiment. ICs are clustered in 10-min windows, where the light waveforms are averaged waveform over 20 sweeps and dark ones are 10 min (300-sweep) averages. The time frames have been chosen unevenly with higher resolution at the beginning when the most dramatic changes took place and lower resolution towards the end when the signals were relatively stable. Signals are standardized to [0, 1] for the emphasis of waveform at various times instead of amplitude.
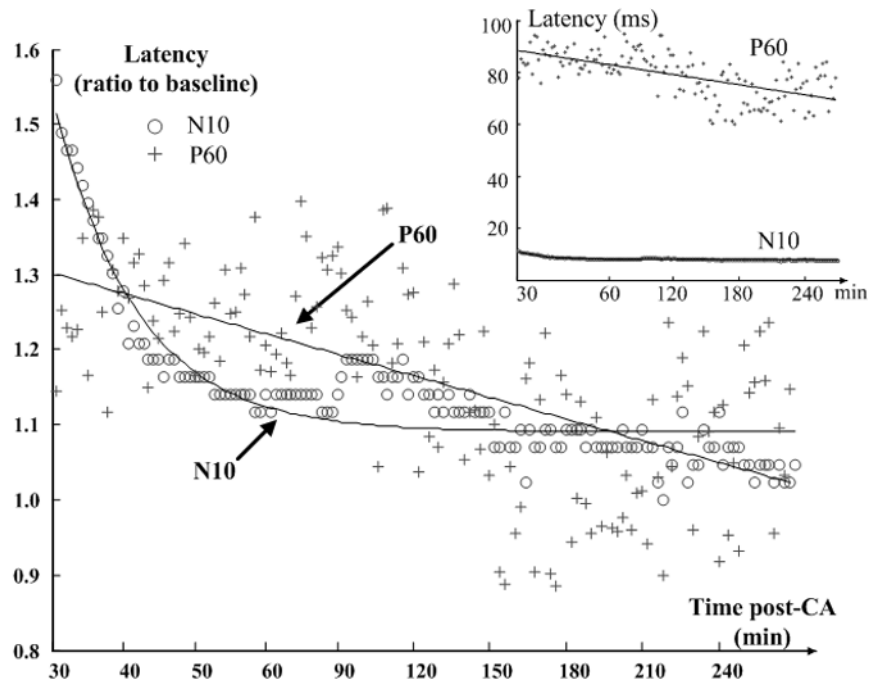
Fig. 4.
Evolution of N10 and P60 latencies during the initial four hours of recovery after CA. Latencies are measured on 20-sweep averages, where the SL-peak N10 is from IC1 and LL-peak P60 is from IC2. Timeframes are 10min-long and are continuous for the first hour but intermittent for the next three hours. In the main plot, latencies are normalized to baseline for comparison, whereas the inset shows the absolute values. The N10 trend is fitted by an exponential line and the P60 trend follows the linear regression.